Proceedings of the 14th International Middle East Power Systems Conference (MEPCON'10), Cairo University, Egypt, December 19-21, 2010, Paper ID 295.

Improvement of Energy-Capturing Efficiency in Stand-alone Photovoltaic Systems with Battery Storage

O. E. M. Youssef, N. M. B. Abdel-Rahim, A. Shaltout

Faculty of Engineering at Shoubra, Benha University, Cairo, Egypt

Faculty of Engineering, Cairo University, Giza, Egypt

omsamoh@yahoo.com nabdelrahim@gmail.com aashaltout@yahoo.com

***Abstract*- Stand-alone photovoltaic systems supplying remote houses have storage battery banks. The battery banks improve the reliability of these residential systems. There is a maximum-voltage limit of the battery bank to protect it against overcharging. Maintaining the battery-bank voltage at its maximum limit is accompanied with reduction of captured energy from the renewable energy source. In this paper, stand-alone residential PV system is studied. Control technique for a motor driving water pump is developed such that the problem of reduction of captured power is reduced. Experimental setup is constructed in the laboratory to verify the performance of the system.**

I. INTRODUCTION

Renewable energy sources, such as photovoltaic (PV) and wind energy are used by stand-alone systems supplying remote houses. These sources are of intermittent nature and, therefore, the stand-alone systems include storage battery banks. The storage battery banks improve the reliability of these systems because the excess energy is stored in the battery banks, and this energy is delivered to the load when the available energy is not sufficient.

The general configuration of stand-alone residential PV system is shown in Fig. 1 [1]–[4]. There is a maximum voltage limit of the battery bank to protect the battery bank against overcharging. Also, there is a minimum voltage limit (or final discharge voltage), which is considered to prevent the over discharging of the battery bank and, therefore, to ensure its maximum life time [1], [5]–[7]. It is required to capture the maximum power from the PV energy source provided that the maximum voltage limit is not exceeded [1].

Maintaining the battery-bank voltage at its maximum limit is usually accompanied with reduction of captured energy from the renewable energy source. Different solutions are suggested to solve the problem of reduction of captured power [8]. These solutions are based on increasing the size of the battery storage, making the maximum voltage value as a function of the charge rates or connecting loads such as pumping loads and heating loads when the battery bank voltage is near its maximum value. However, increasing the size of the battery storage is costly solution, and using variable values for the maximum voltage may lead to overcharging of the battery bank. On the other hand, connecting loads near maximum voltage value needs simple control.

In this paper, stand-alone residential PV system is studied. Control technique for a permanent-magnet DC (PMDC) motor driving water pump is developed such that the problem of reduction of captured power is reduced.

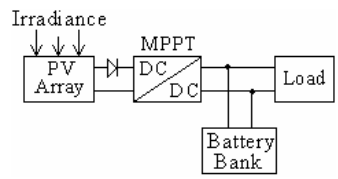

Fig. 1 Stand-alone residential PV system
(MPPT is abbreviation of Maximum Power Point Tracking).

Experimental setup is constructed in the laboratory to verify the performance of the system.

II. CHARACTERISTICS OF PV ARRAY

The PV array consists of parallel-connected strings with each string consisting of a number of series-connected modules. Each PV module consists of series connected PV cells [2], [9]. The dependency of the current–voltage characteristics of the PV array on solar radiation (G) is shown in Fig. 2. The corresponding power–voltage characteristics are also shown together with the maximum power points [10].

III. SYSTEM CONTROL

There are different MPPT techniques to obtain maximum power operation of PV array. In this paper, direct maximum-power-point tracking (DMPPT) technique is used [11]. In this method, the duty ratio (D) of the MPPT converter is controlled by directly using the output power of the PV array (P_g). The condition of maximum power point which is tracked by the control of the MPPT converter is

$$\frac{dP_g}{dD} = 0 \tag{1}$$

The duty ratio is increased or decreased periodically, according to the values of ΔP_g and ΔD, to move the operating point toward the maximum power point.

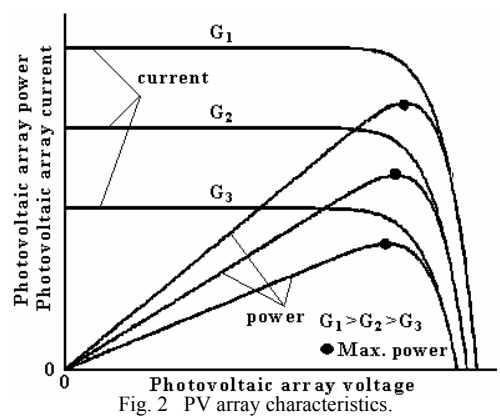

Fig. 2 PV array characteristics.

As mentioned above, the battery-bank voltage must be taken into account to protect the battery bank against overcharging. According to the battery-bank voltage (u_{dc}), we have two modes of operation. Mode 1 is when $u_{dc} \leq U_{max}$, and Mode 2 is when $u_{dc} > U_{max}$, where U_{max} is the maximum voltage limit of the battery bank. Fig. 3 illustrates these operating modes. When the voltage u_{dc} is increased beyond U_{max} , the relationship ($u_{dc} = U_{max}$) is maintained by decreasing the captured power. The captured power is decreased according to the values of ΔP_g and ΔD, to move the operating point away from the maximum power point.

IV. MOTOR-LOAD CONTROL

The motor is driving water pump. To control the motor without conflict with water demand, the system must have water tank, Fig. 4. Here, the water tank is divided into two parts, low part and high part. The low part is small compared to high part, and the motor must operate to fill up this part with water to guarantee continuous water supply. For the high part of water tank, the motor is operated near maximum DC-bus voltage to fill up this part with water. This leads to increase the captured power near maximum DC-bus voltage. The water tank is provided with two switches to detect water level, low switch (SWL) and high switch (SWH). Each of these switches is of ON state when the water level is below the switch level, and is of OFF state when the water level reaches the switch level. The modes of control of PMDC motor are determined according to states of these switches and the value of the DC-bus voltage as follows:

A. Mode I of Motor Control

This mode of operation takes place when SWL is ON and, hence, SWH is ON (see Fig. 4). This means that the low part of the water tank is not completely filled with water. As a result, the duty ratio of the converter controlling the motor is increased gradually when the DC-bus voltage is above the U_{min} value and is decreased gradually when the DC-bus voltage is below the U_{min} value, where U_{min} is the minimum voltage limit of the battery bank.

B. Mode II of Motor Control

This mode takes place when SWL is OFF, SWH is ON, and the DC-bus voltage is near its maximum value. This means that the low part of water tank is completely filled with water. In this mode, a preset voltage value (U_{PRESET}) near maximum voltage limit is used by motor control. The duty ratio of the converter controlling the motor is increased when the DC-bus voltage is higher than U_{PRESET}, and is decreased when the DC-bus voltage is lower than U_{PRESET} .

C. Mode III of Motor Control

In this mode, the motor is not operated, and this might be due to

(1) SWL is OFF and SWH is OFF. This means that the high part of water tank is completely filled with water.
(2) SWL is OFF and SWH is ON, and DC-bus voltage is lower than U_{PRESET}.
(3) SWL is ON and DC-bus voltage is lower than U_{min} .

The Modes of control of PMDC motor converter are shown in Fig. 5. The system configuration with controlled PMDC motor is shown in Fig. 6, where i_{BAT} is the battery-bank current, i_M is the motor current and ω_m is the motor speed.

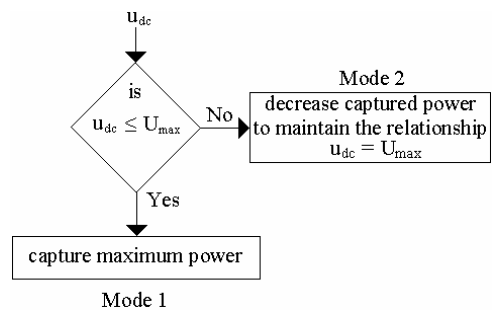

Fig. 3 Modes of operation.

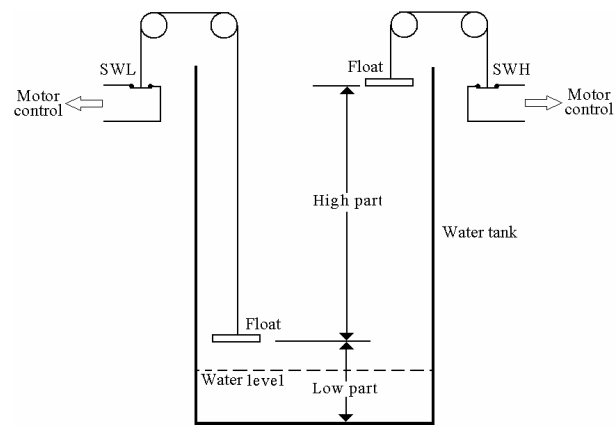

Fig. 4 Water tank with two switches operated according to the water level.

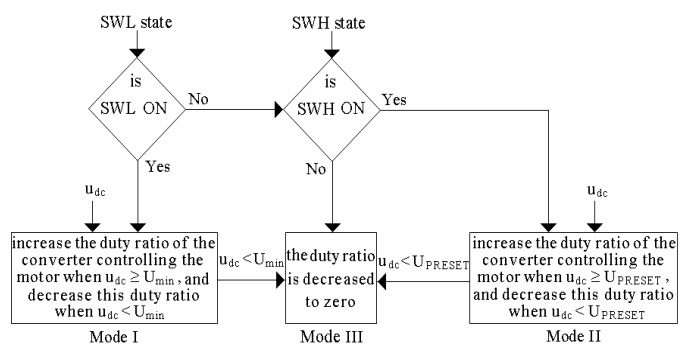

Fig. 5 Modes of control of PMDC motor converter.

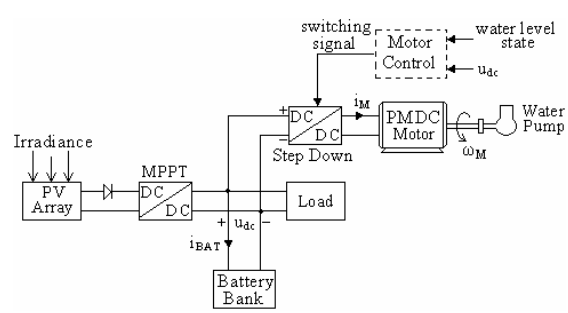

Fig. 6 Residential PV system with controlled PMDC motor load.

V. EXPERIMENTAL SETUP

In the laboratory, the source of light was realized by tungsten-halogen (quartz-halogen) lamps [9], [12]. The experimental setup has one PV module of the characteristics given in Appendix I. To calculate the rated power of halogen lamps that gives the rated-output power of the PV module, we have

$$\text{efficiency} = \frac{\text{output power}}{\text{input power}}$$

$$\text{(efficiency of lamps).(efficiency of PV module)} = \frac{\text{rated power of PV module}}{\text{rated power of lamps}} \quad (2)$$

The rated power of PV module is equal to 120 watt. Taking the efficiency of halogen lamps equal to 10 % and the efficiency of PV module equal to 15 % , the rated power of halogen lamps is equal to 8 kW. The characteristics of the PV module as obtained in the laboratory are shown in Figs. 7 and 8. Fig. 8 shows that the maximum power of PV module is less than its rated power. This is due to the aging of the PV module, and due to some light is falling far from the surface of the PV module.

PMDC motor driving air blower is used as the system motor load. A controlled DC-power supply parallel with a dump resistance and large capacitor is used instead of the battery bank as shown in Fig. 9. The dump resistance is used to ensure that the current is always coming out of the DC power supply, and the large capacitor is used to reduce the voltage ripple of the DC supply.

The control of the PV system and the control of the motor-load, shown in Fig. 6, are implemented using the dSPACE board (DS1104) which is hosted in a PC [13]. This board is a complete real-time control system based on 250 MHz processor. It is used for rapid prototyping of high-speed multivariable digital controllers and real-time simulations. There are 100-pin I/O (Input/Ouput) connectors on the board. An adapter cable connects these pins to a connection panel. Some pins of the board is provided with A/D converters and D/A converters. These pins can be accessed from the connection panel via BNC connectors.

The experimental setup is shown in Fig. 10. A fan is used to ventilate the PV module due to the large heat generated from the halogen lamps. The MPPT along with the PMDC motor control algorithms are loaded into the dSPACE board using MATLAB/SIMULINK. The dSPACE board has input signals of the PV module current (I_g), PV module voltage (U_g), DC-bus voltage (u_{dc}), DC-supply current (i_{BAT}) and motor current (i_M). These signals are obtained by using voltage and current sensors. Also, there is an input signal represent the motor speed (n_M), and this signal is obtained by using tachometer. In addition, there are two input signals represent the status of the switches SWL and SWH. The signals I_g , U_g and u_{dc} are used to control the PV module as described in Section III. Also, the signals of SWL/SWH and the signal u_{dc} are used to control the PMDC motor as described in Section IV. There are two output signals to control the MPPT converter and the step-down DC/DC converter through drive circuits.

The value of dump resistance is 10 Ω and the value of the capacitor bank is 30 mF. The voltage values set by the control scheme are U_{min}= 20 V, U_{max}= 26 V and U_{PRESET} = 25 V.

VI. RESULTS

The complete data of the experiment are given in Appendix I. Results for motor control changed from Mode III to Mode I are shown in Figs. 11 to 15. The water level is reduced suddenly from high part of water tank to low part of water tank, and the DC-bus voltage is below the preset value (25 V). These results are taken at open-circuit voltage of DC supply equal to 32.3 V and internal resistance of DC supply equal to 4.1 Ω, R_L of 20 Ω, SWL is turned on at t = 1.9 s, and include captured power, DC-bus voltage, battery-bank current, motor speed and motor current. Fig. 11(a) shows that maximum power extraction of the PV module takes place because the DC-bus voltage is less than its maximum limit, Fig. 12(a).

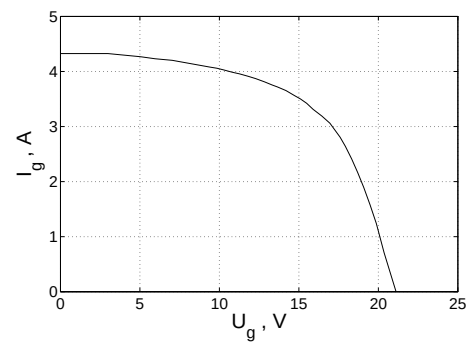

Fig. 7 Current-voltage characteristics of PV module using halogen lamps as light source.

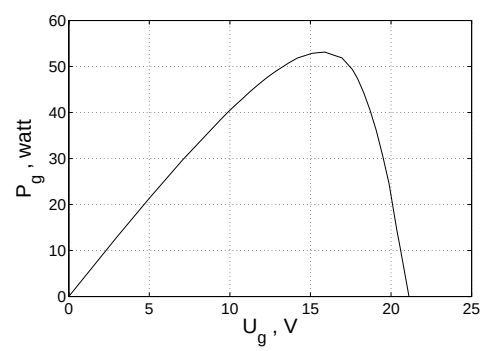

Fig. 8 Power-voltage characteristics of PV module using halogen lamps as light source.

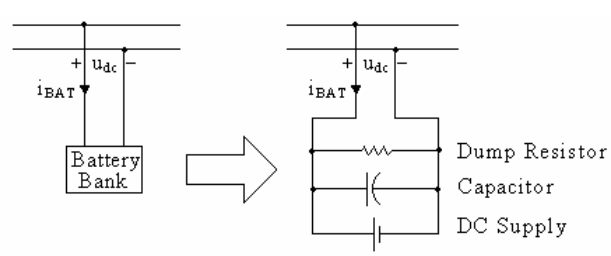

Fig. 9 DC supply combination that used instead of battery bank.

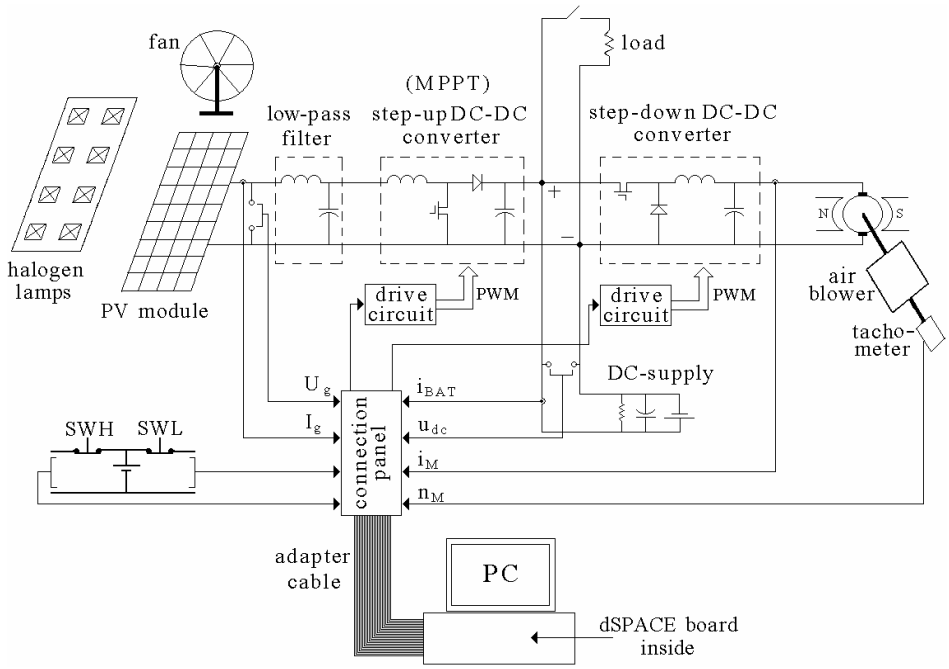

Fig. 10 Experimental setup.

Fig. 14(a) shows that the motor speed is increased gradually from zero to the steady-state value. Fig. 15(a) shows that the motor current is increased gradually from zero to the steady-state value. Fig. 12(a) shows that the DC-bus voltage is decreased gradually by the gradual increasing of the motor current. Fig. 13(a) shows that the battery-bank current is changed gradually from charging (positive) current to discharging (negative) current by the gradual increasing of the motor current. The system is simulated using MATLAB/SIMULINK [14]. The figures show good agreement between experimental and simulation results.

Results for motor control during Mode III (i.e. the motor is not operated) are shown in Figs. 16 and 17. These results are taken at open-circuit voltage of DC supply equal to 33 V and internal resistance of DC supply equal to 4.1 Ω, SWL is OFF and SWH is OFF (i.e. water tank is completely filled with water), and include captured power and DC-bus voltage. During Mode III, disconnection of R_L makes the control to reduce the captured power from the PV array, Fig. 16, to limit the DC-bus voltage, Fig. 17, at its maximum limit (26 V).

Results for motor control changed from Mode III to Mode II are shown in Figs. 18 to 21. These results are taken at open-circuit voltage of DC supply equal to 33 V and internal resistance of DC supply equal to 4.1 Ω, SWL is OFF and SWH is ON. The results include captured power, DC-bus voltage, motor speed and motor current. Changing from Mode III to Mode II has taken place due to disconnection of R_L. The disconnection of R_L has the effect of increasing the DC-bus voltage above its preset value, Fig. 19. To keep the DC-bus voltage from exceeding its maximum value, the captured power from the PV module is reduced, Fig. 18. The motor speed, Fig. 20, is increased gradually until the DC-bus voltage becomes near the U_{PRESET} value (25 V). Increasing of the motor speed is associated with increasing of the captured power until maximum power operation is obtained. Fig. 21 shows that the motor current is increased gradually from zero to steady-state value.

Results for motor control changed from Mode II to Mode III are shown in Figs. 22 to 25. These results are taken at open-circuit voltage of DC supply equal to 33 V and internal resistance of DC –supply equal to 4.1 Ω, SWL is OFF and SWH is ON. The results include captured power, DC-bus voltage, motor speed and motor current. Changing from Mode II to Mode III has taken place due to connection of R_L. Connection of the resistance leads to reduce the DC-bus voltage below the U_{PRESET} value, Fig. 23. Therefore, the motor speed, Fig. 24, is decreased gradually to zero. Fig. 22 shows peak-power operation of PV array because the DC-bus voltage is less than the maximum limit. Fig. 25 shows that the motor current is decreased gradually to zero.

Results for motor control changed from Mode III to Mode I are shown in Figs. 26 to 29. The water level is reduced suddenly from high part of water tank to low part of water tank, where the DC-bus voltage is below the preset value (25 V). These results are taken at open-circuit voltage of DC supply equal to 22.9 V and internal resistance of DC supply equal to 4.1 Ω, SWL is turned on at t = 2.23 s, and include captured power, DC-bus voltage, motor speed and motor current. Fig. 26 shows that maximum power extraction of the PV module takes place because the DC-bus voltage is less than its maximum limit. The motor speed, Fig. 28, is increased gradually until the DC-bus voltage becomes near the U_{min} value (20 V), Fig. 27. Fig. 29 shows that the motor current is increased gradually from zero to the steady-state value. Fig. 27 shows that the DC-bus voltage is decreased gradually by the gradual increasing of the motor current.

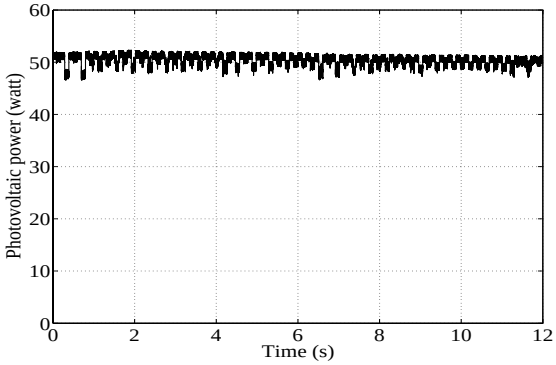

(a) experimental result

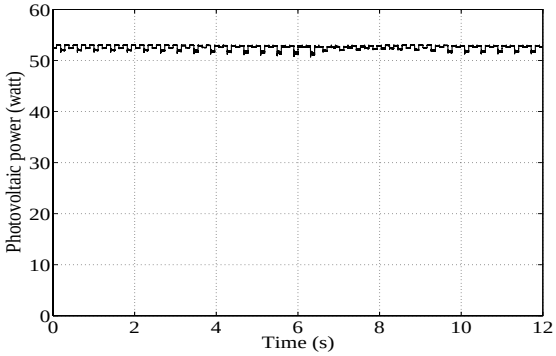

(b) simulation result

Fig. 11 Captured power for $R_L = 20\ \Omega$ and motor control changed from Mode III to Mode I at time of about 1.9 s.

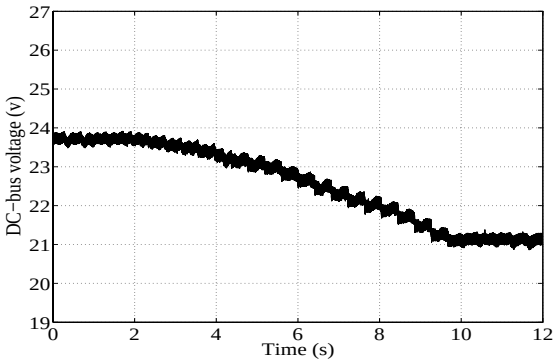

(a) experimental result

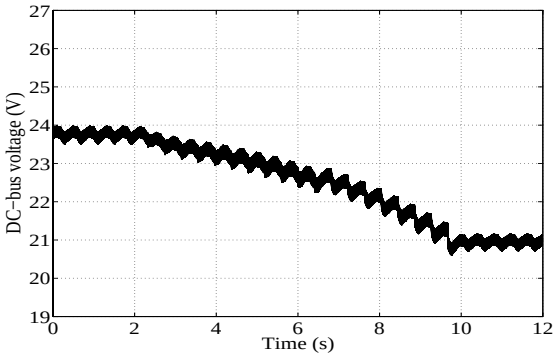

(b) simulation result

Fig. 12 DC-bus voltage for $R_L = 20\ \Omega$ and motor control changed from Mode III to Mode I at time of about 1.9 s.

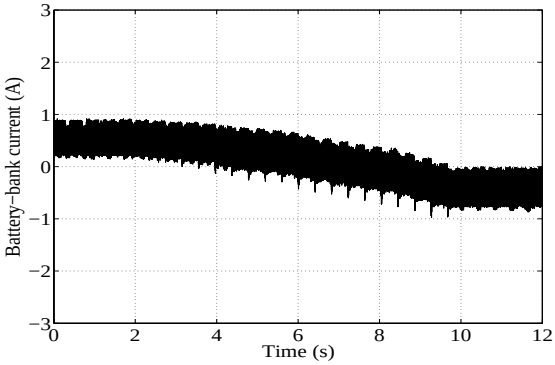

(a) experimental result

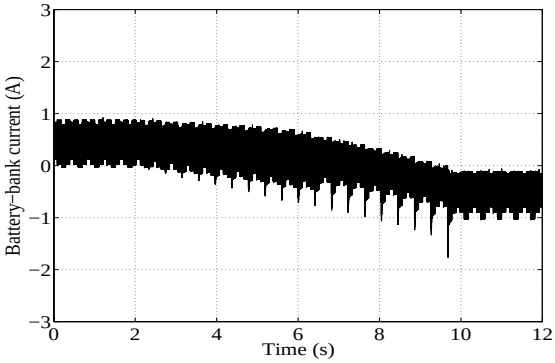

(b) simulation result

Fig. 13 Battery-bank current for $R_L = 20\ \Omega$ and motor control changed from Mode III to Mode I at time of about 1.9 s.

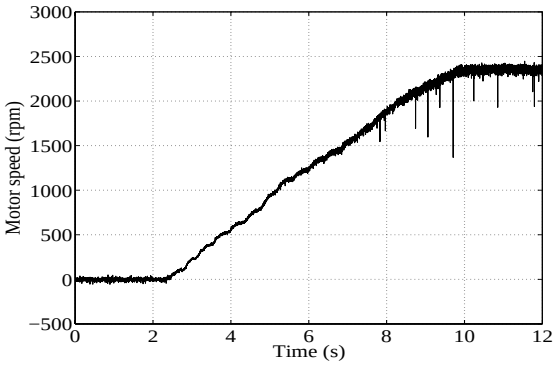

(a) experimental result

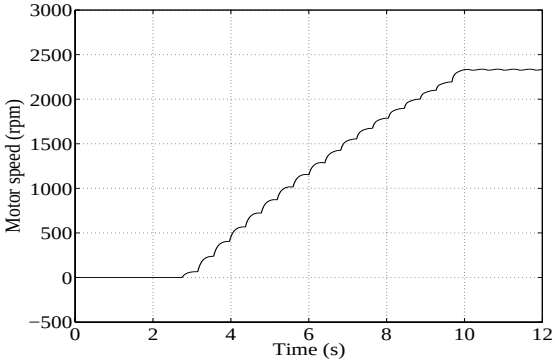

(b) simulation result

Fig. 14 Motor speed for $R_L = 20\ \Omega$ and motor control changed from Mode III to Mode I at time of about 1.9 s.

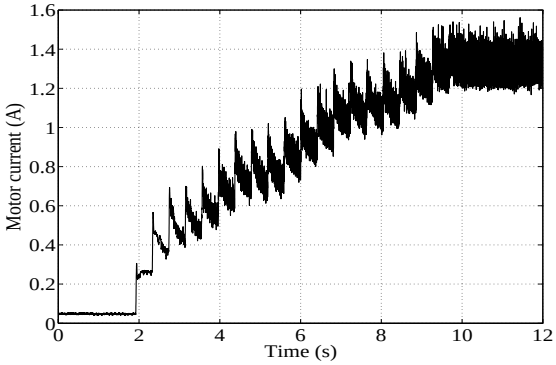

(a) experimental result

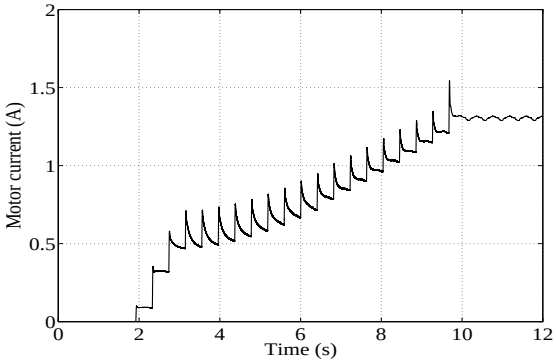

(b) simulation result

Fig. 15 Motor current for $R_L = 20\ \Omega$ and motor control changed from Mode III to Mode I at time of about 1.9 s.

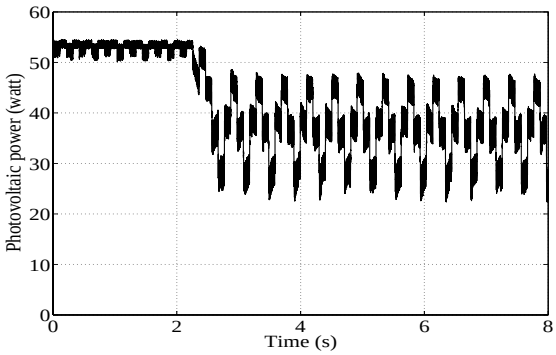

Fig. 16 Captured power during Mode III (i.e. motor is not operated) where R_L of 20 Ω is disconnected at about 2.25 s.

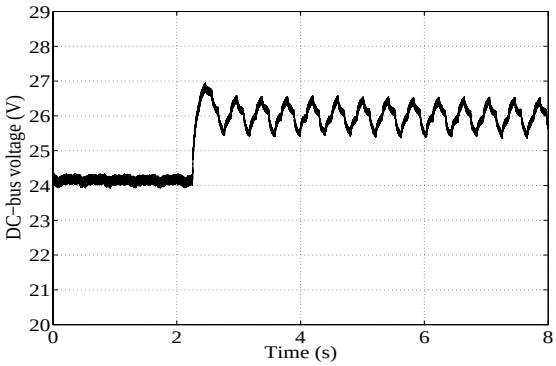

Fig. 17 DC-bus voltage during Mode III (i.e. motor is not operated) where R_L of 20 Ω is disconnected at about 2.25 s.

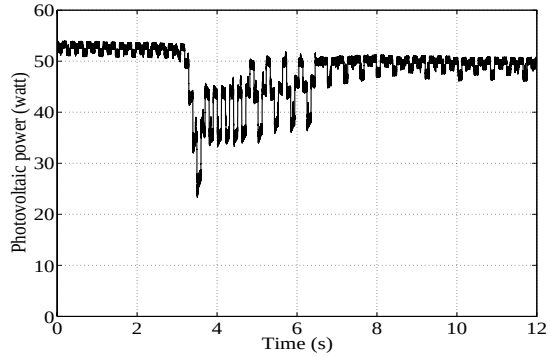

Fig. 18 Captured power for SWL is OFF, SWH is ON, motor control changed from Mode III to Mode II due to disconnection of R_L equal to 20 Ω at time of about 3 s.

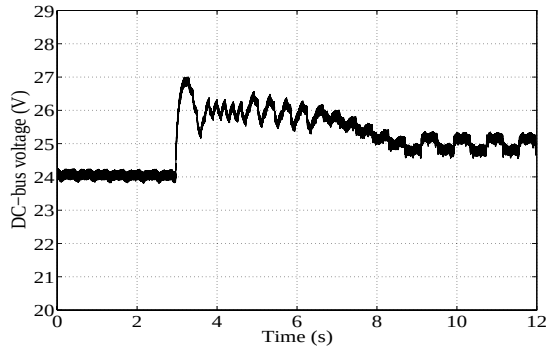

Fig. 19 DC-bus voltage for SWL is OFF, SWH is ON, motor control changed from Mode III to Mode II due to disconnection of R_L equal to 20 Ω at time of about 3 s.

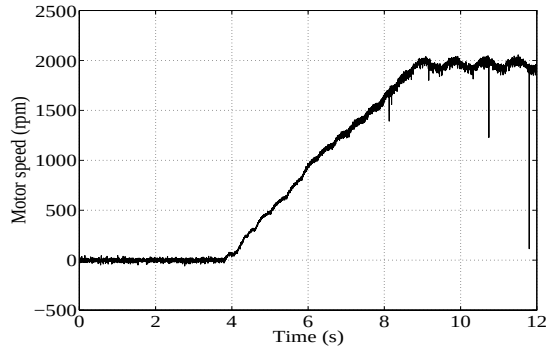

Fig. 20 Motor speed for SWL is OFF, SWH is ON, motor control changed from Mode III to Mode II due to disconnection of R_L equal to 20 Ω at time of about 3 s.

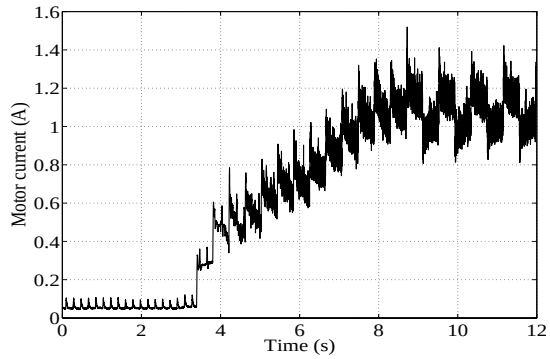

Fig. 21 Motor current for SWL is OFF, SWH is ON, motor control changed from Mode III to Mode II due to disconnection of R_L equal to 20 Ω at time of about 3 s.

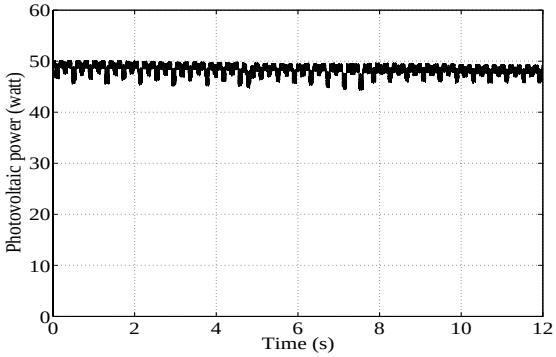

Fig. 22 Captured power for SWL is OFF, SWH is ON, motor control changed from Mode II to Mode III due to connection of R_L equal to 20 Ω at time of about 4.6 s.

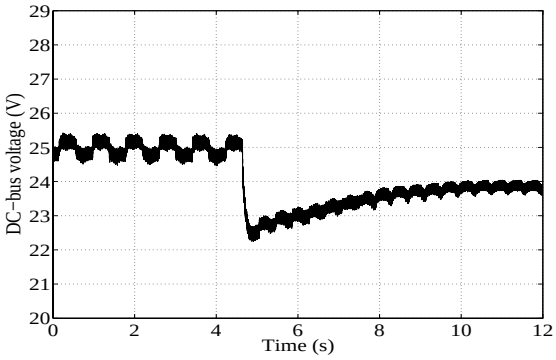

Fig. 23 DC-bus voltage for SWL is OFF, SWH is ON, motor control changed from Mode II to Mode III due to connection of R_L equal to 20 Ω at time of about 4.6 s.

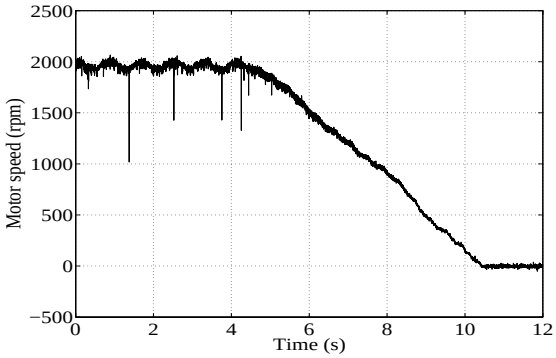

Fig. 24 Motor speed for SWL is OFF, SWH is ON, motor control changed from Mode II to Mode III due to connection of R_L equal to 20 Ω at time of about 4.6 s.

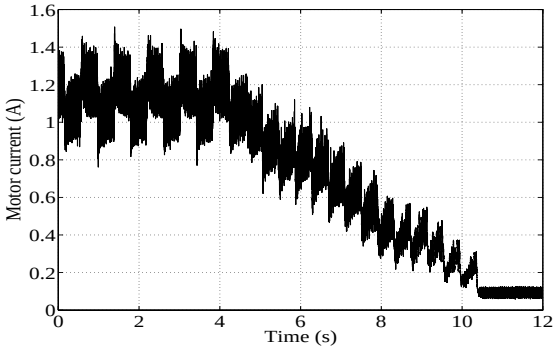

Fig. 25 Motor current for SWL is OFF, SWH is ON, motor control changed from Mode II to Mode III due to connection of R_L equal to 20 Ω at time of about 4.6 s

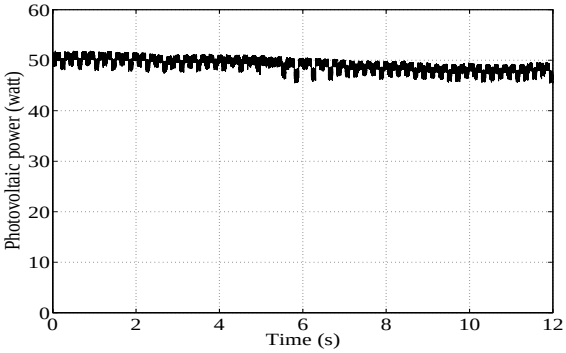

Fig. 26 Captured power for motor control changed from Mode III to Mode I at time of about 2.23 s.

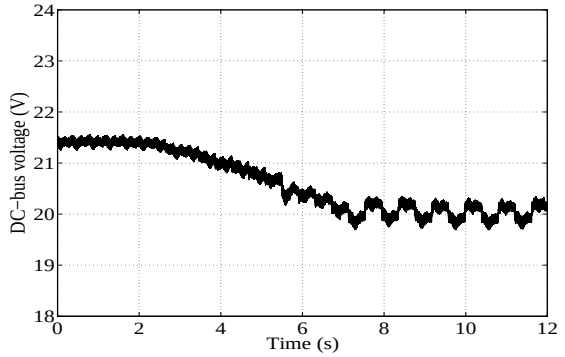

Fig. 27 DC-bus voltage for motor control changed from Mode III to Mode I at time of about 2.23 s.

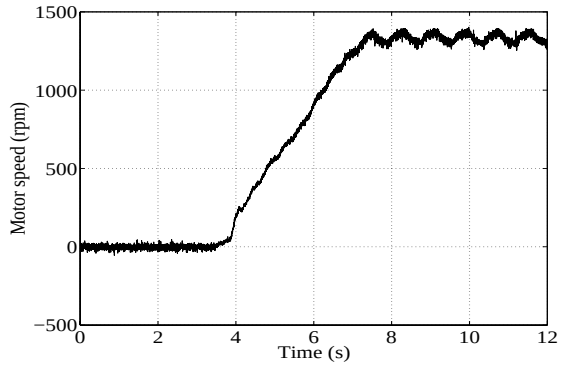

Fig. 28 Motor speed for motor control changed from Mode III to Mode I at time of about 2.23 s.

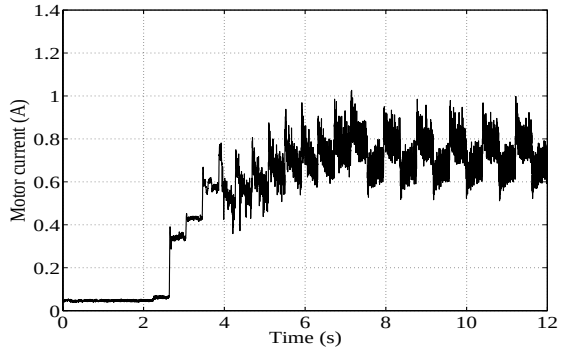

Fig. 29 Motor current for motor control changed from Mode III to Mode I at time of about 2.23 s.

CONCLUSION

Stand-alone systems have the problem of reduction of the captured energy near maximum-voltage limit of the battery bank. This voltage limit is considered to protect the battery bank against overcharging. Stand-alone residential PV system is studied. Control technique for a permanent-magnet DC (PMDC) motor driving water pump is developed such that the problem of reduction of captured power is reduced. The system has water tank to control the motor without conflicting with water demand. Experimental setup is constructed in the laboratory to verify the performance of the system. The control of the PV system and the control of the motor-load are implemented using the dSPACE board (DS1104) which is hosted in a PC. Experimental results show good agreement with predicted results.

REFERENCES

[1] B. S. Borowy and Z. M. Salameh, "Dynamic response of a stand-alone wind energy conversion system with battery energy storage to a wind gust," IEEE Trans. Energy Conversion, vol. 12, no. 1, pp. 73─78, March 1997.

[2] T. Markvart, "Solar electricity," Book, John Wiley & Sons, 1995.

[3] E. S. Gavanidou and A. G. Bakirtzis, "Design of a stand alone system with renewable energy sources using trade off methods," IEEE Trans. Energy Conversion, vol. 7, no. 1, pp. 42─48, March 1992.

[4] M. G. Jaboori, M. M. Saied, and A. A. R. Hanafy, "A contribution to the simulation and design optimization of photovoltaic systems," IEEE Trans. Energy Conversion, vol. 6, no. 3, pp. 401─406, Sep. 1991.

[5] E. Koutroulis and K. Kalaitzakis, "Design of a maximum power tracking system for wind-energy-conversion applications," IEEE Trans. Ind. Electron., vol. 53, no. 2, pp. 486─494, April 2006.

[6] M. H. Nehrir, B. J. LaMeres, G. Venkataramanan, V. Gerez, and L. A. Alvarado, "An approach to evaluate the general performance of stand-alone wind/photovoltaic generating systems," IEEE Trans. Energy Conversion, vol. 15, no. 4, pp. 433─439, Dec. 2000.

[7] J. P. Dunlop, "Batteries and charge control in stand-alone photovoltaic systems, fundamentals and application," Report, Sandia National Laboratories, Photovoltaic systems Applications Dept., Jan. 1997.

[8] D. Corbus, C. Newcomb, E. I. Baring-Gould, and S. Friedly, "Battery voltage stability effects on small wind turbine energy capture," National Renewable Energy Laboratory (NREL), US, May 2002.

[9] K. K. Tse, B. M. T. Ho, H. S.-H. Chung, and S. Y. R. Hui, "A comparative study of maximum-power-point trackers for photovoltaic panels using switching-frequency modulation scheme," IEEE Trans. Ind. Electron., vol. 51, no. 2, pp. 410─418, April 2004.

[10] J. H. R. Enslin, M. S. Wolf, D. B. Snyman, and W. Swiegers, " Integrated photovoltaic maximum power point tracking converter," IEEE Trans. Ind. Electron., vol. 44, no. 6, pp. 769─773, Dec. 1997.

[11] E. Koutroulis, K. Kalaitzakis, and N. C. Voulgaris, "Development of a microcontroller-based, photovoltaic maximum power point tracking control system," IEEE Trans. Power Electron., vol. 16, no. 1, pp. 46─54, Jan. 2001.

[12] "Photovoltaic engineering, experimental module system," ELWE, March 2002, http://www.elwe.com

[13] http://www.dspace.com

[14] SIMULINK 7, The MathWorks, Inc., 2007.

APPENDIX I

A. PV-Module Characteristics

The PV module is GP120 module and has the following specifications:

Maximum power = 120 watt,
Voltage at maximum power = 16.9 V,
Current at maximum power = 7.1 A,
Open-circuit voltage = 21 V,
Short-circuit current = 7.7 A,
and the current–Voltage characteristics of the PV at different insolation levels and cell temperature of 25° C are shown in Fig. 30.

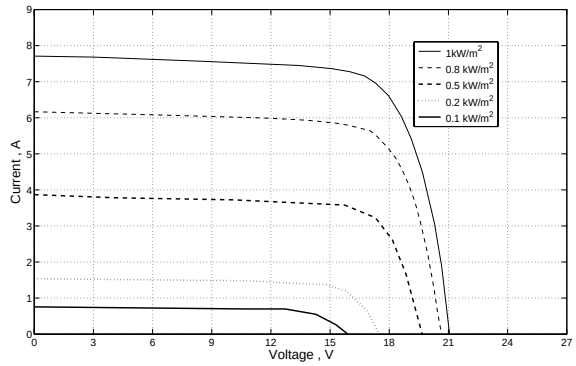

Fig. 30 PV module characteristics at different insolation levels.

B. Data of step-up DC-DC converter

Inductance = 6 mH, capacitance = 4.7 mF and switching frequency = 0.98 kHz.

C. Data of low-pass filter

Inductance = 2 mH, capacitance = 330 μF.

D. Data of step-down DC-DC converter

Inductance = 6 mH, capacitance = 5.4 mF and Switching frequency = 0.98 kHz.

E. Data of DC motor and its load

The motor is 24 V PMDC motor, and has the following parameters:

$R_a = 4\ \Omega$, $L_a = 0.0001$ H, $C_e = 0.0611$ V.s/ rad and

The load torque is given by:

$T_L = 0.0287 + 8.561 \times 10^{-7}\ \omega_M^2$ N.m

Inertia of the motor and its load (J_M) = 7.843×10^{-5} Kg.m^2